Supplementary Information

Collectively optimized Pt-O bond and morphology engineering of structurally ordered Pt_3Zn intermetallic for high-efficiency zinc-air devices

Chenzhong Wu and Qingmei Wang*

School of Chemistry and Chemical Engineering, Guizhou University, Guiyang 550025, China.

* Corresponding author. E-mail: qmwang3@gzu.edu.cn (Q. M. Wang).

Experimental Section

Materials

Zinc (II) acetylacetonate hydrate ($Zn(acac)_2$, analytical pure 97%), Hexadecyl trimethyl ammonium bromide (CTAB), Platinum (II) acetylacetonate ($Pt(acac)_2$, analytical pure 98%), Oleyl amine (OAm) and Ethanol (CH_3CH_2OH) were purchased from Aladdin. Glucose($C_6H_{12}O_6$) and Cyclohexane(C_6H_{12}) were obtained from Macklin. The Vulcan XC-72 carbon-supported 20% commercial Pt catalyst was sourced from Johnson Matthey. All chemicals utilized were commercially available and were used as received without additional purification. Ultra-pure water was produced utilizing an HHitech purification system on a resistance of 18.25 MΩ/cm and used in all experimental procedures.

Synthesis of Pt_3Zn nanocubes nanoparticles

A flask contained 7 mL of oleyl amine was charged with 2.2 mg of $Zn(acac)_2$, 32 mg of hexadecyl trimethyl ammonium bromide, 10 mg of $Pt(acac)_2$ and 60 mg of glucose. The resulting mixture was subjected to sonication for 1 hour to ensure uniform dispersion of the precursors in the oleyl amine solvent, facilitating the subsequent reaction. The sonicated homogeneous solution was then putted into an oil-bath pot and heated additive to 160 °C for 8 hours. Upon cooling to room temperature, the solution underwent centrifugation with a 1: 8 cyclohexane/ethanol mixture to take out residual oleyl amine excessive agents from the surface. The centrifuged product was dispersed in 10 mL of 5% acetic acid and stirred at 80 °C for 12 hours, further achieving a surface Pt-rich structure. Ultimately, the product Pt_3Zn NCs nanoparticles were acquired under the operation of washing and centrifugation.

Electrocatalysis material synthesis of Pt_3Zn NCs

The synthesized Pt_3Zn NCs nanoparticles were loaded onto Vulcan XC-72 carbon black to evaluate the electrochemical performance and characterize the physical properties. Vulcan XC-72 carbon black support serves both as an electrical conductor and a support material. The Pt_3Zn NCs and carbon black (model number: Vulcan XC-72) were stirred in a 20 mL cyclohexane/ethanol solution for 12 hours to form Pt_3Zn NCs catalyst. The resulting product was collected after drying via centrifugation and was subsequently used for electrochemical testing and physical characterization.

Characterization

The TEM images, HAADF-STEM, and energy-dispersive spectroscopy (EDS) were obtained by a JEM ARM200F equipped with a cold field-emission gun and aberration corrector microscope at 200 kV acceleration voltage. The nanoparticle sizes were measured with Nano measurer 1.2 software, and the total number of particles in this statistic is 100. The XPS analysis was carried out using a Kratos AXIS Ultra DLD XPS (Kratos Analytical). The XPS system is equipped with a monochromatic Al Kα source operated at 15 keV and 150 W, a hemispherical analyzer, a charge neutralizer, a catalysis cell, and a load lock chamber for the rapid introduction of samples without breaking the vacuum. X-rays were incident at an angle of 45° with respect to the surface normal. Analysis was performed at a pressure of $\sim 1 \times 10^{-9}$ mbar and high-resolution core level spectra were measured with a pass energy of 40 eV. The XPS experiments were performed using an electron beam, directed to the sample, for charge neutralization. In-situ reduction of the materials was performed in a reaction cell (Model: ES-009R01) directly attached to the XPS chamber, which allows the sample to be treated under gas flow conditions. The samples were transferred inside the reaction cell and back to the analysis chamber without exposure to the atmosphere. All the peaks were adjusted using the C 1s peak at 284.8 eV as the reference. The ICP-OES analysis was manipulated on an Elan DRC-e instrument.

Electrochemical Measurements

Electrochemical analysis was performed in a standard three-electrode system by applying an electrochemical workstation (Donghua test, Dh7003). The standard three-electrode is formed of a working electrode (glassy carbon (GC)), reference electrode (Ag/AgCl), and counter electrode

(carbon rod). All potential, unless mentioned otherwise, were transformed to the reversible hydrogen electrode (RHE). To manufacture the catalyst ink, 2 mg of all as-prepared catalyst was dissolved in the mixed solutions, which contained ethanol (790uL) and Nafion solutions (10 uL), and then ultrasonicated for 0.5 h. Immediately, the 10 uL ink of all as-prepared catalysts was measured by utilizing a pipette and drop-dried onto a working electrode to obtain ~2.5 ug Pt loading (the area of 0.19625 cm^2). The commercial Pt/C catalyst as reference was pursued to similarly process operation. Subsequently, the 10 uL ink of commercial Pt/C catalyst was drop-dried onto a working electrode to obtain ~5 ug Pt loading. The cyclic voltammetry (CV) is carried out by applying cyclic scans between 0.05 to 1.2 V (vs RHE) in fresh N_2-saturated 0.1 M $HClO_4$ electrolyte solutions (sweep rate: 0.05V/s). The oxygen reduction reaction (ORR) analysis is implemented in O_2-saturated 0.1 M $HClO_4$ electrolyte solutions (sweep rate: 0.01V/s; rotating speeds: 1600 rpm). The CO stripping experiments are operated in 0.1M $HClO_4$ electrolyte solutions. The CO gas is bubbled into electrolyte solutions for ~20 min. Then the dissolved CO is purified using high-purity N_2-saturated for 0.5h in the 0.1 M $HClO_4$ electrolyte solutions. The accelerated durability test (ADT) is executed in O_2-saturated 0.1 M $HClO_4$ solutions, and a cyclic potential scan of 40,000 CV cycles is performed at a scanning rate of 50 mV/s between 0.6 and 1.2 V. The cyclic potential scan of commercial Pt/C catalyst was only circulated 30,000 CV cycles at a scanning rate of 50 mV/s between 0.6 and 1.2 V.

The methanol oxidation reaction (MOR) was conducted in an N_2-saturated 0.1M $HClO_4$ solution containing 0.5 M methanol at room temperature. Before electrochemical measurements, all the electrodes were pre-processing by recycling the potential between 0.05 V and 1.2 V vs. RHE at a scan rate of 50 mV s^{-1} for 100 cycles to remove some surface impurity. The test solutions were 0.1 M $HClO_4$ and 0.1 M $HClO_4$ + 0.5 M CH_3OH solutions at room temperature. Chronoamperometry was conducted at an invariable potential of 0.75 V in 0.1 M $HClO_4$ + 0.5 M CH_3OH solution continuously for 10000 s.

The ethanol oxidation reaction (EOR) was conducted in an N_2-saturated 0.1 M $HClO_4$ solution containing 0.5 M ethanol at room temperature. Chronoamperometry was conducted at an invariable potential of 0.75V in 0.1 M $HClO_4$ + 0.5 M CH_3CH_2OH solution continuously for 10000 s.

According to the peak area of CO stripping and the loading of Pt on the electrode, we calculate the electrochemical surface area (ECSA) of the catalysts via the following equation:

$$ECSA_{CO}=Q_{CO}/(0.42*[Pt]) \quad (1)$$

$$j_K=(j_d*j)/(j_d-j) \quad (2)$$

$$MA=(j_k*1000)/(0.19625*[Pt]) \quad (3)$$

$$SA=MA/ECSA_{CO} \quad (4)$$

Q_{CO} refers to the electric quantity calculated by the integral of CO stripping peak. The [Pt] refer to the loading quantity of Pt on the electrode (mg/cm^2). The j is the current density at 0.9V and j_d is the limit current density under test conditions. The 0.19625 is the area of the glassy carbon electrode (cm^2)

The electron transfer number (n) was gained from the ORR polarization curves tested with different rotating speeds from 625 to 2500 rpm, using Koutecky-Levich first order:

$$j^{-1}=j_K^{-1}+j_L^{-1}=j_L^{-1}+B^{-1}\omega^{-1/2} \quad (5)$$

where $B = 0.2nFD_0^{2/3}C_0v^{-1/6}$. In eq (5), j is the measured current density, which consists of kinetic (j_K) and diffusion-limiting current (j_L); B is a constant; ω is the rotation speed in rpm; F is the Faraday constant (96485 C/mol); n is the number of electrons transferred per oxygen molecule; C_0 is the bulk concentration of O_2 (1.5×10^{-3} mol/L in 0.1 M $HClO_4$); D_0 is the diffusion coefficient for O_2 in 0.1 M $HClO_4$ (2.0×10^{-5} cm^2/s); and v is the kinetic viscosity of the solution (0.01 cm^2/s). A constant of 0.2 was used for B when the unit of rotation speed is given in rpm.

Zinc-air devices measurement

A homemade aqueous zinc-air battery (ZABs) was employed for the evaluation of the battery performance. A polished zinc foil was used as the anode, and a hydrophilic carbon fiber paper substrate coating with the catalyst layer (1 mg cm^{-2}) was used as the air cathode. The

mixed solution of 6.0 M KOH+0.2 M Zn $(AC)_2 \cdot 2H_2O$ was used as the electrolyte in the alkaline zinc-air batteries (ZABs). Measurements were performed on a CHI 760 electrochemical workstation at room temperature. The LSV polarization curve measurements were performed at 10 mV s^{-1}. The galvanostatic charge and discharge were performed at room temperature by a LAND testing system at 5 mA cm^{-2} with 10 min of discharge followed by 10 min of charge. The flexible all-solid-state ZABs assembly Polyvinyl alcohol (PVA, 3 g) powder was dissolved in 30 mL deionized water at 95 °C under magnetic stirring for about 2 h. Then, 3.0 mL of 18.0 M KOH solution containing 0.2 M Zn $(Ac)_2 \cdot 2H_2O$ was added to the above solutions, followed by stirring at 95 °C for 1 h to form a homogeneous gel. The obtained gel was poured onto a glass plate to form a thin film and frozen at -3 °Cover 12 h, then thawed at room temperature naturally. Finally, the solid-state electrolyte was obtained. The polished Zn foil and Pt_3Zn NCs based air electrode were placed on opposite sides of the polymer hydrogel electrolyte as the anode and cathode. For comparison, the alkaline and neutral Pt/C based ZABs were assembled by using the mixture of commercial Pt/C catalyst (loading of 1 mg cm^{-2}) as the air electrode.

DFT computational details

Spin-plorized density functional theory (DFT) calculations were performed within the Vienna Ab-Initio Simulation Package (VASP)[1,2]. The projector augmented wave (PAW) [3] method was used to describe the ionic cores. And the electron exchange-correlation was modelled by Perdew-Burke- Ernzerhof (PBE) function within generalized gradient approximation (GGA)[4]. A plane-wave basis set with cutoff energy of 450 eV was used to describe the valence electrons[5]. The convergence criterion was 10^{-5} eV for energy and 0.02eV/Å for force. And the (2 × 2 × 1) Monkhorst–Pack k-point meshes were set for k-space integration. The four atomic and (4×4) Pt (111) slab modle was constructed to simulate Pt (111) surface. And Pt_3Zn (111) model was created by cleaving the (111) surface of Pt_3Zn cell which contain four atom layers and 64 atoms. An 18 Å vacuum was added to all slab to prevent artificial interactions in the z-direction. Atoms in the bottom two metal layers were kept fixed during the geometry optimization in the slab calculations.

The Gibbs free energy G of each species was calculated as follow:

$$G = E + ZPE - TS$$

where G, E, ZPE and TS are the free energy, total energy from DFT calculations, zero-point energy and entropic contributions (T was set to be 300K), respectively. ZPE and TS could be derived after frequency calculation. Then free energy of the reaction (ΔG) can be obtained by subtracting the total free energy of the products from that of the reactants. Besides, the adsorption energy (ΔE_{ad}) of intermediates were calculated according to

$$\Delta E_{ad} = E_{ads+sur} - E_{ads} - E_{sur}$$

$E_{ads+sur}$, E_{ads}, E_{sur} are the energy of surface with adsorbate, single adsorbate, and surface respectively.

Supplementary Schemes

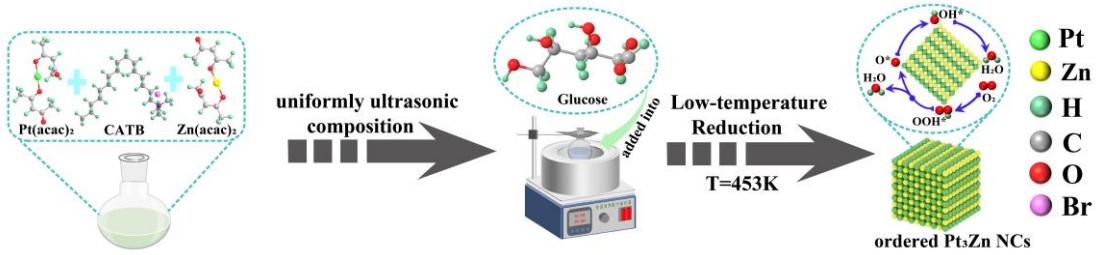

Scheme S1. Schematic illustration of the main steps for fabricating structurally ordered Pt_3Zn NCs catalysts.

Supplementary Figures

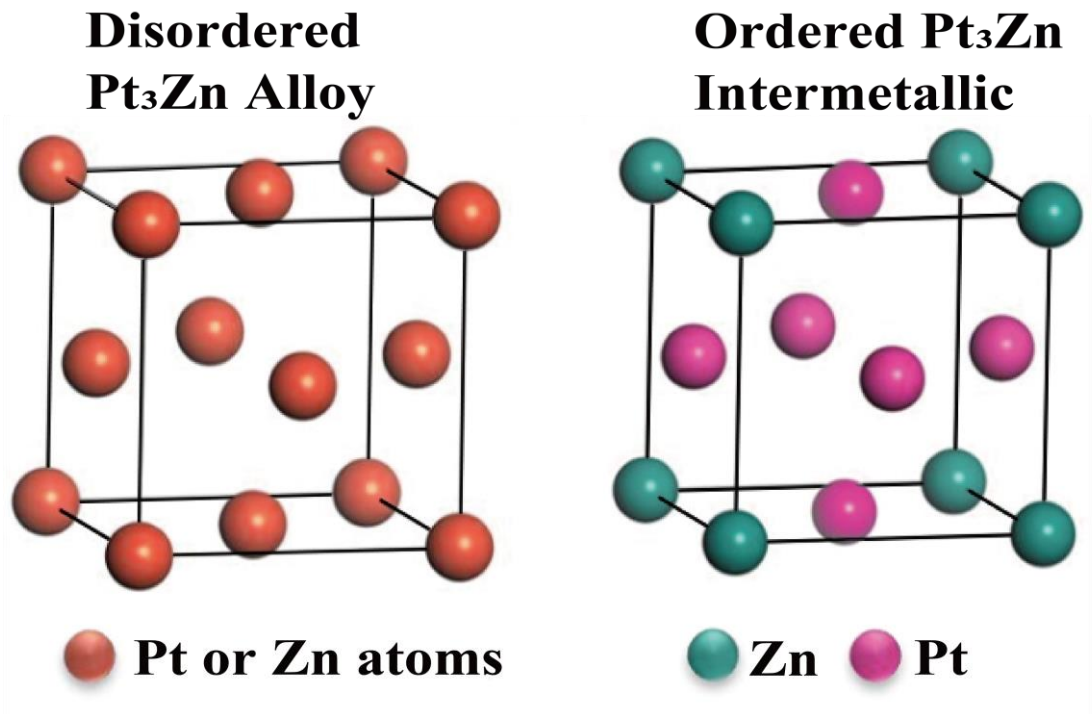

Fig. S1. The unit-cell structure simulation of disordered Pt_3Zn model (a) and structurally ordered intermetallic $L1_2$ Pt_3Zn NC catalyst (b).

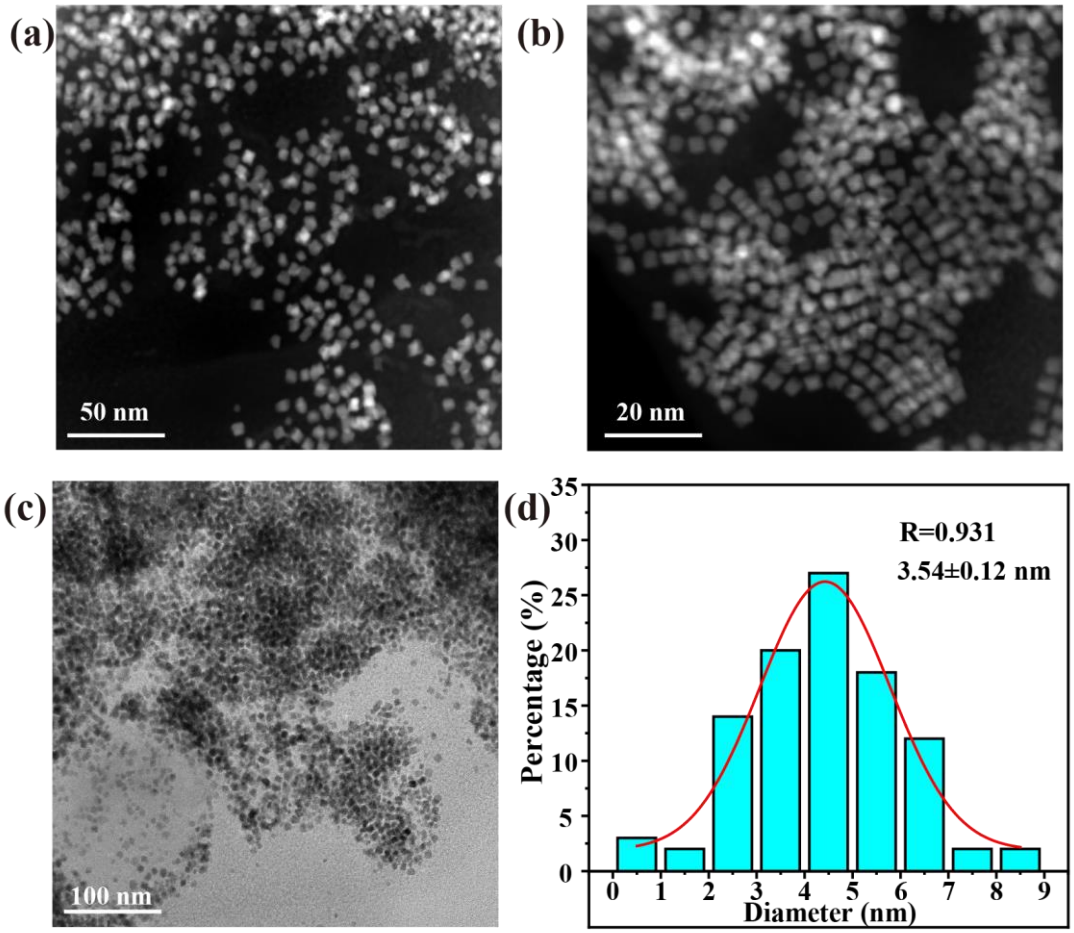

Fig. S2. (a)TEM images and (b) corresponding particle size distribution of Pt_3Zn NCs sample catalyst. (c,d) HAADF STEM images on Pt_3Zn NCs at various magnifications, exhibiting nanoparticle features a well- definite nanocubes morphology.

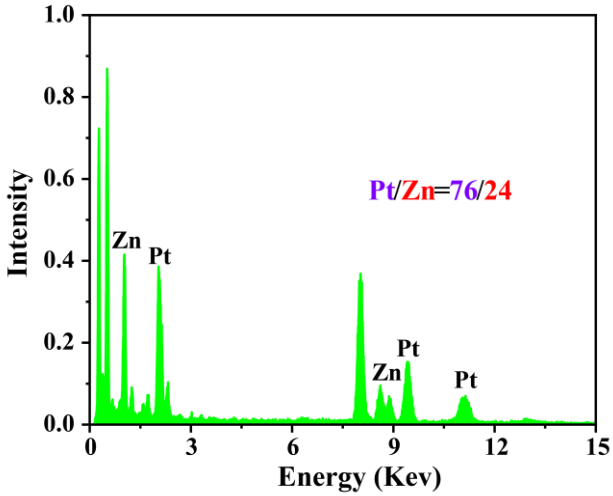

Fig. S3. EDS spectrum of corresponding element mapping.

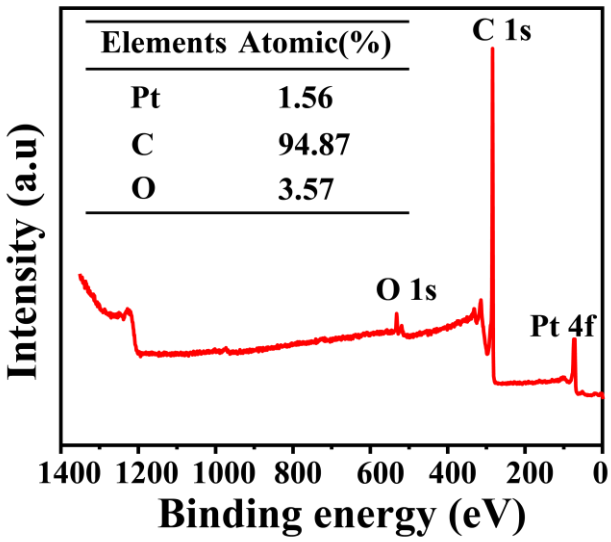

Fig. S4. The XPS survey spectrum of commercial Pt/C catalyst. We could observe the characteristic signal of Pt 4f, C 1s, and O1s elements, which further confirmed the presence of Pt, C, and O elements in Pt/C catalysts.

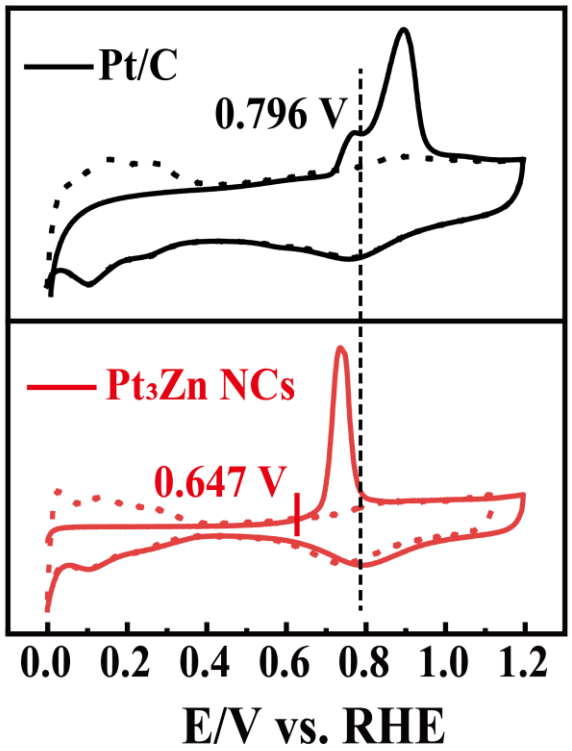

Fig. S5. A comparison of CO stripping voltammograms for Pt_3Zn NCs and Pt/C in 0.1 M $HClO_4$.

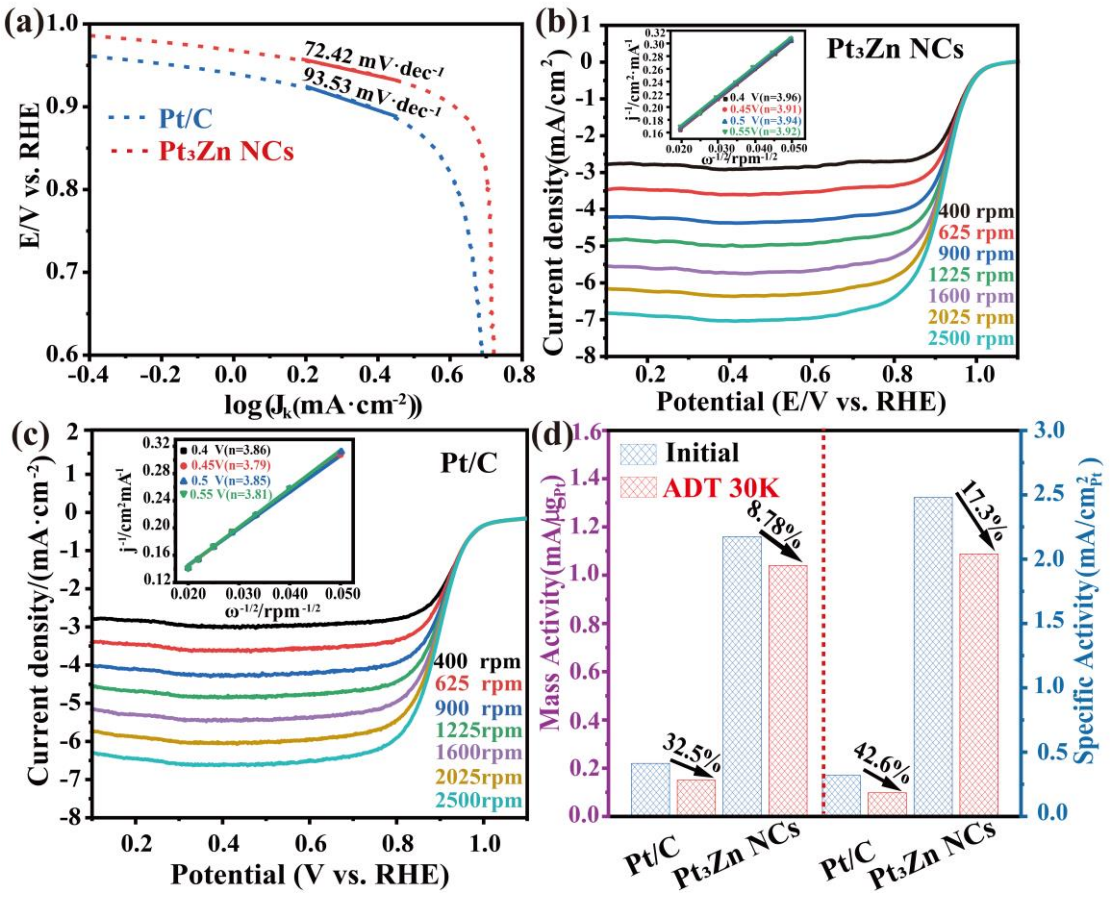

Fig. S6. (a) The Tafel slope curves of Pt_3Zn NCs sample and Pt/C. ORR polarization curves of commercial Pt/C catalysts (b) and (c) at various rotation rates as well as Koutecky-Levich plots at various electrode potentials(inset). (d) The loss of MA and SA of Pt_3Zn NCs sample and Pt/C catalysts.

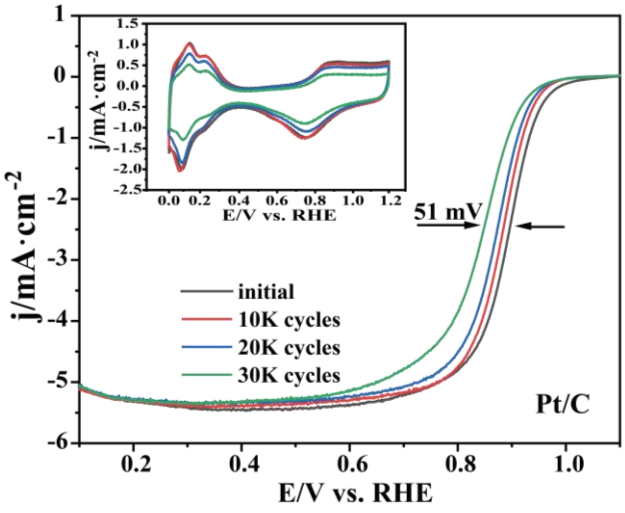

Fig. S7. ORR polarization curves of commercial Pt/C catalysts at long-term operation durability (inset: the CV curves of commercial Pt/C catalysts). The accelerated durability test was carried out by applying 10,000~30,000 CV potential sweeps cycles between 0.6 and 1.1V VS. RHE in O_2-saturated 0.1 M $HClO_4$ at a scan rate of 50mV·s^{-1}.

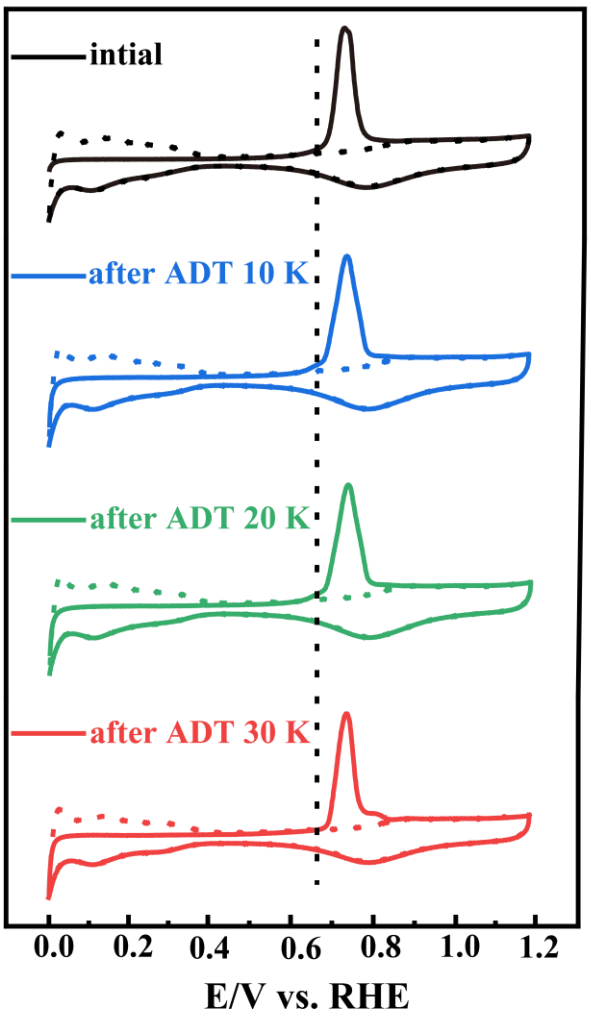

Fig. S8. CO stripping experiments of Pt_3Zn NCs sample before and after ADT.

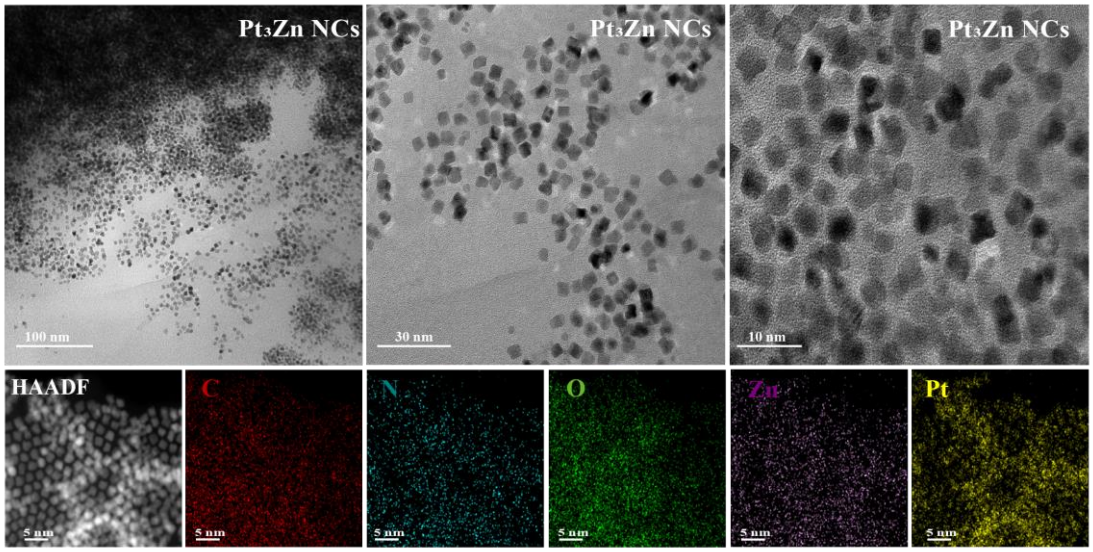

Fig. S9. The TEM (a-c) and (d-i) HAADF-STEM image of Pt_3Zn NCs after 30000 cycles.

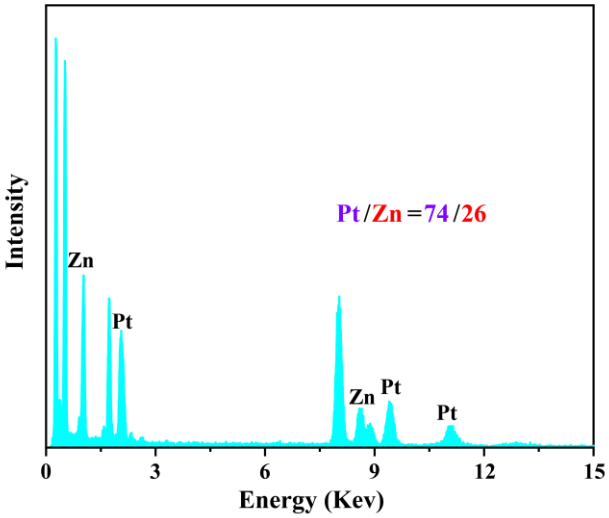

204

205 **Fig. S10.** EDS spectrum of corresponding element mapping after ADT 30,000 potential circles.

206

207

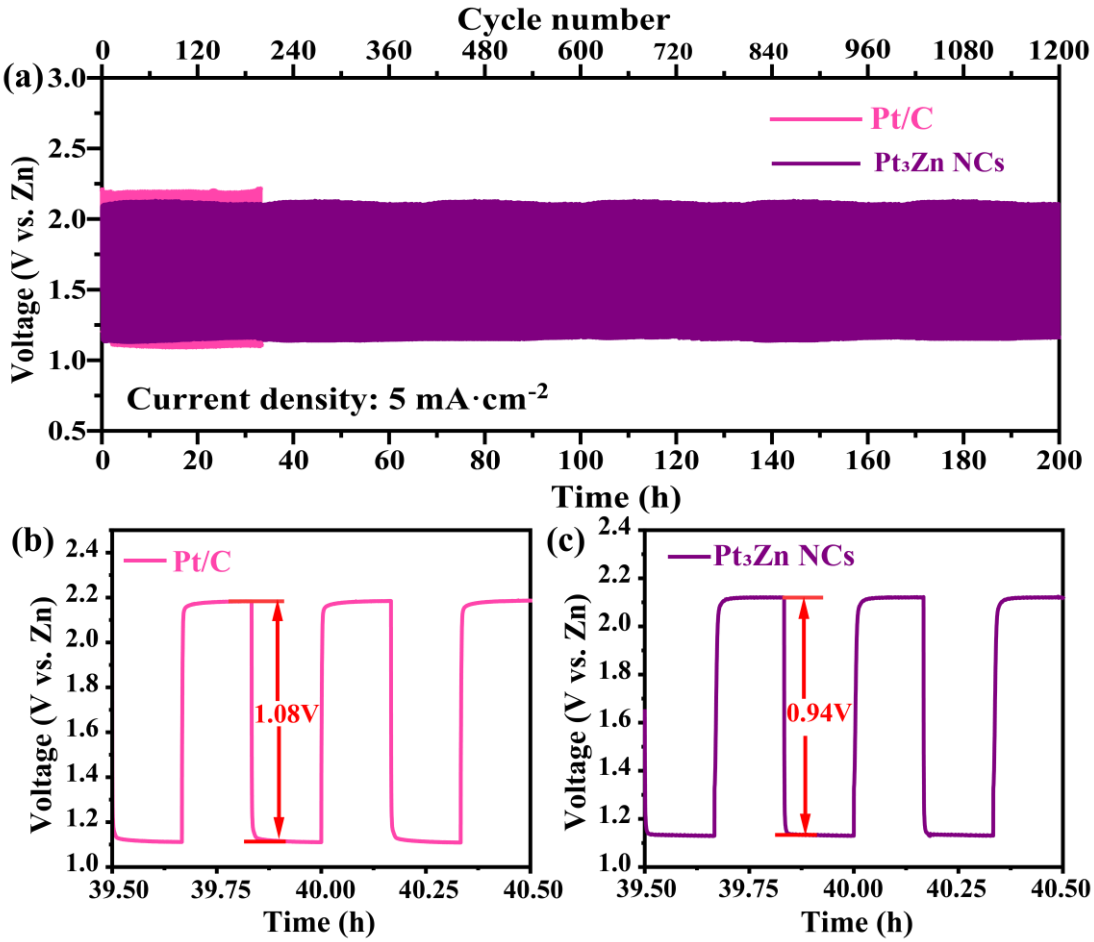

Fig. S11. (a) Performance during galvanostatic cycling. Partial diagram of constant current charge-discharge at 40 hours for Pt/C (b) and Pt_3Zn NCs (c) catalyst.

Flexible all-solid-state ZABs

Fig. S12. Image of a red LED illuminated by the flexible all-solid-state ZABs.

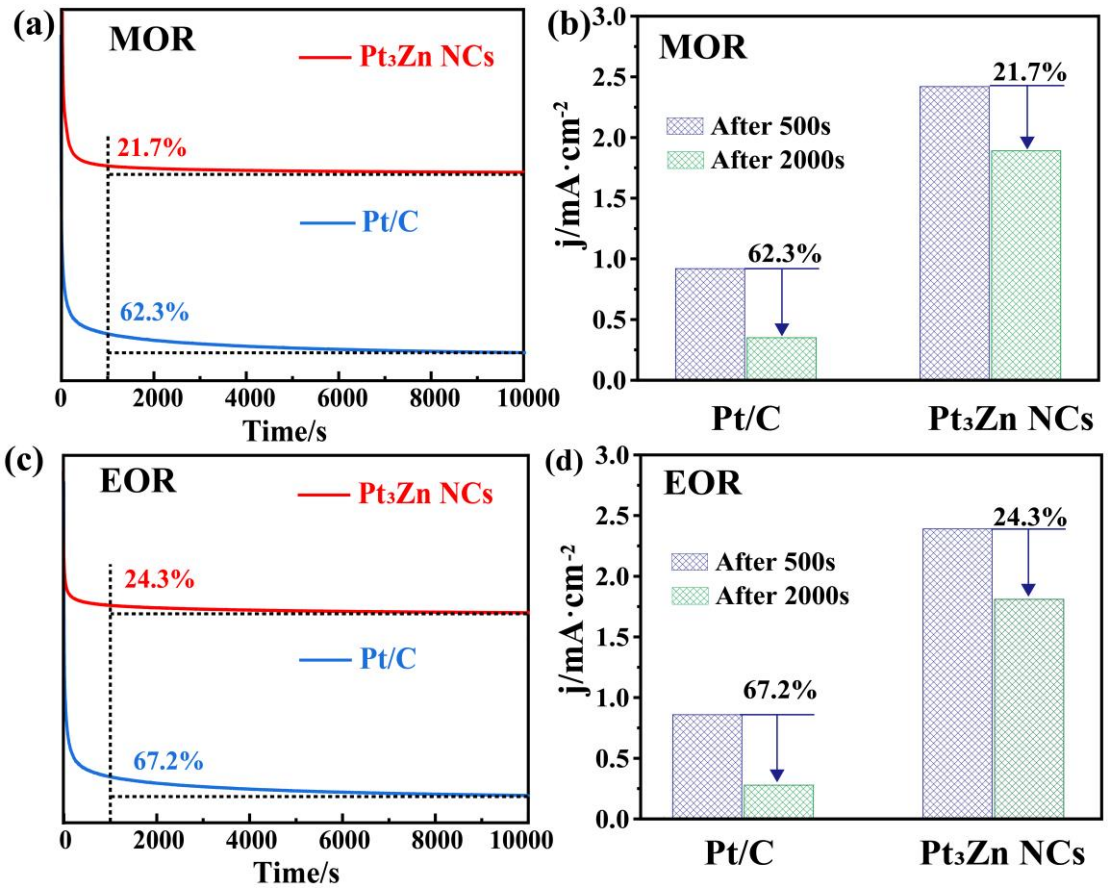

Fig. S13. The CA tests for Pt_3Zn NCs samples and Pt/C at 0.75 V for MOR (a) and EOR (c). The chronoamperometry (CA) in 0.1M $HClO_4$ + 0.5 M CH_3OH (b) and 0.1 M $HClO_4$ + 0.5 M CH_3CH_2OH (b) solution under a constant potential of 0.75 V vs RHE for 10000 s. The commercial Pt/C catalyst showed a more substantial decline compared to the initial values, with 62.3% and 67.2% reductions in current density for MOR and EOR.

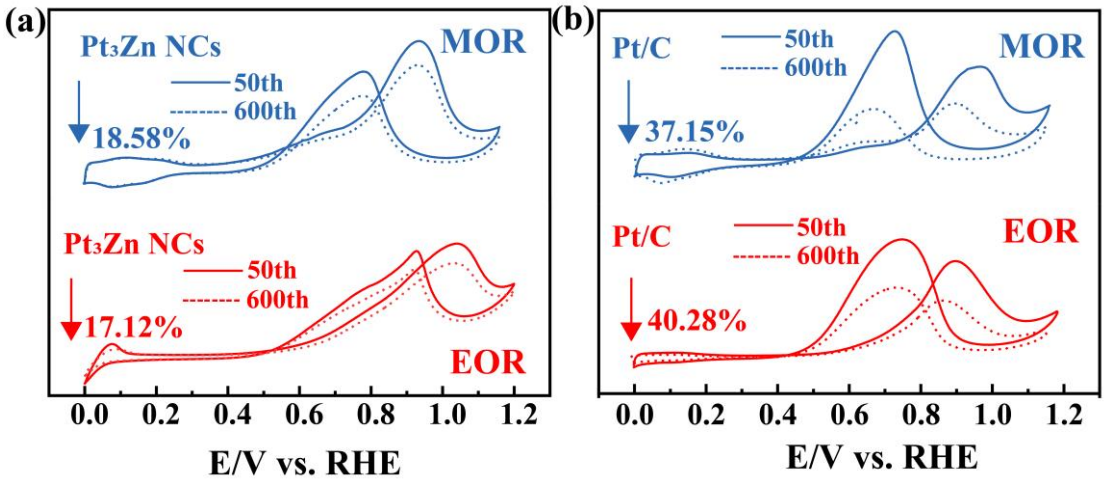

Fig. S14. Cyclic voltammogram of the Pt_3Zn NCs samples (a) and Pt/C catalyst (b) before and after 600 cycles durability test in N_2-saturated 0.1 M $HClO_4$ + 0.5 M CH_3OH solution for MOR and 0.1 M $HClO_4$ + 0.5 M CH_3CH_2OH solution for EOR.

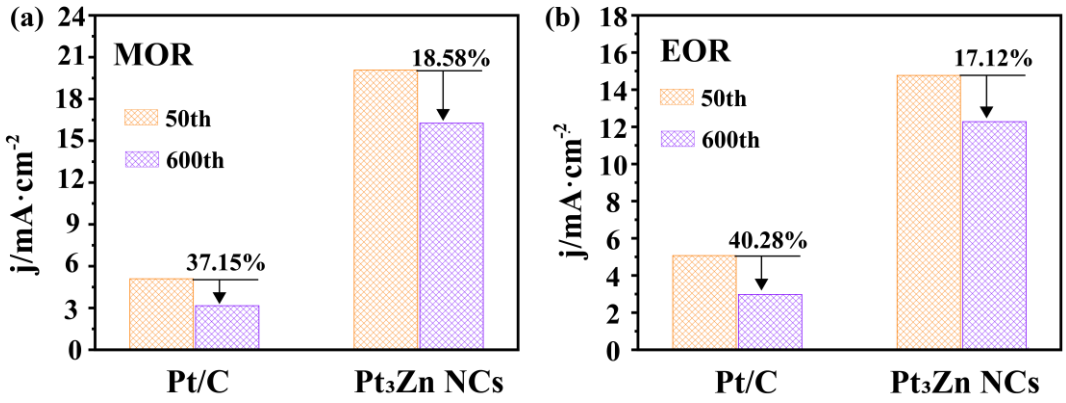

Fig. S15. The current density rate of decline comparison histogram of Pt_3Zn NCs catalysts and commercial Pt/C before and after 600 cycles durability tests in N_2-saturated 0.1 M $HClO_4$ + 0.5 M CH_3OH solution for MOR (a) and 0.1 M $HClO_4$ + 0.5 M CH_3CH_2OH solution for EOR (b).

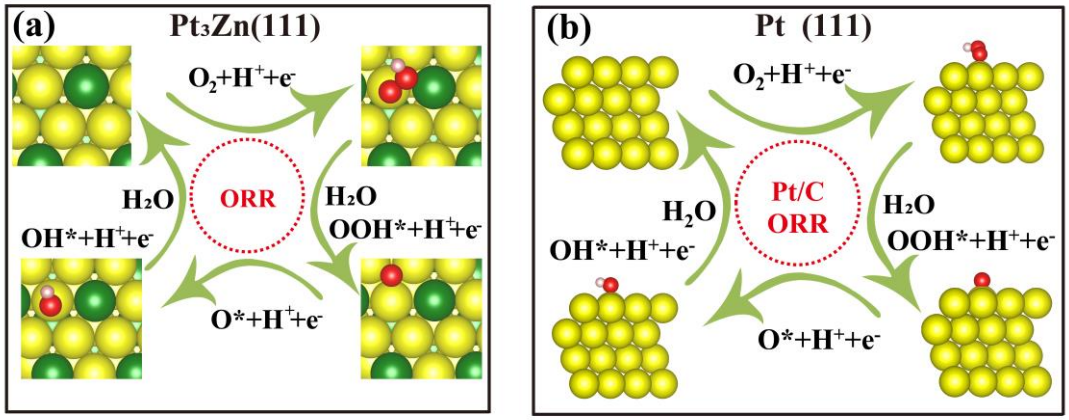

Fig. S16. Scheme of the pathway in ORR mechanism of Pt3Zn NCs model (a) and Pt (111) of Pt/C catalyst (b) based on DFT.

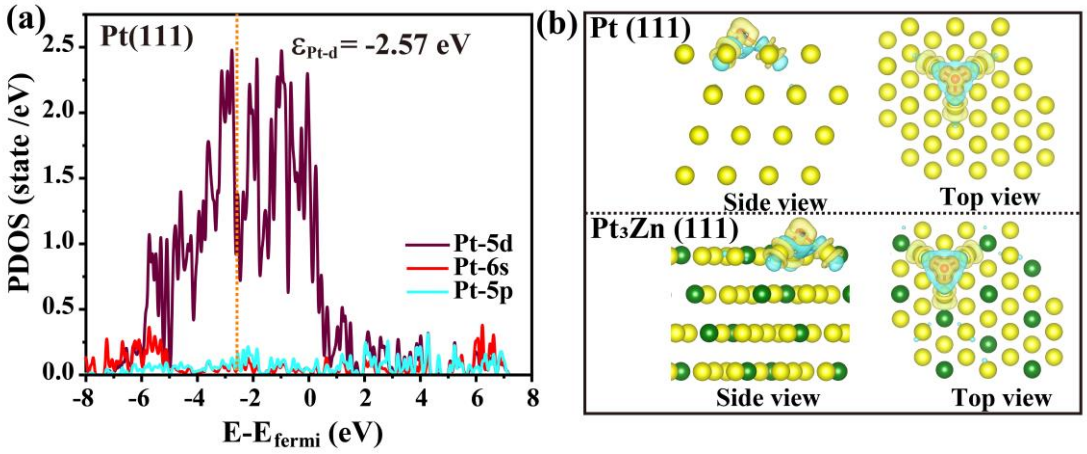

Fig. S17. The PDOS on Pt/C catalyst. (b) CDD of Pt (111) (top) and Pt_3Zn (111) (bottom).

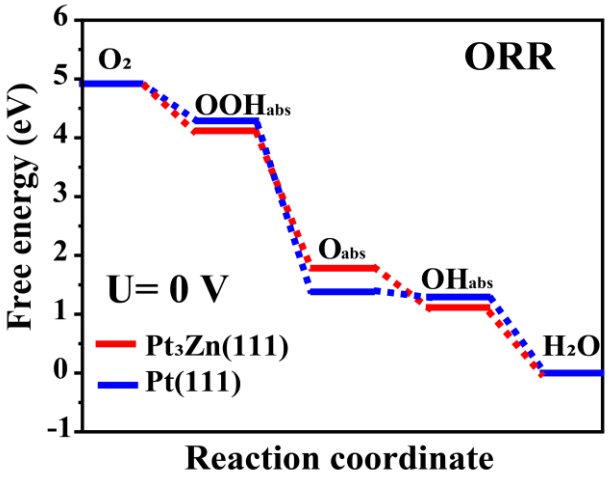

Fig. S18. Gibbs free energy step diagram of the ORR pathways at the 0 V voltage for Pt (111) of Pt_3Zn NCs sample for DFT.

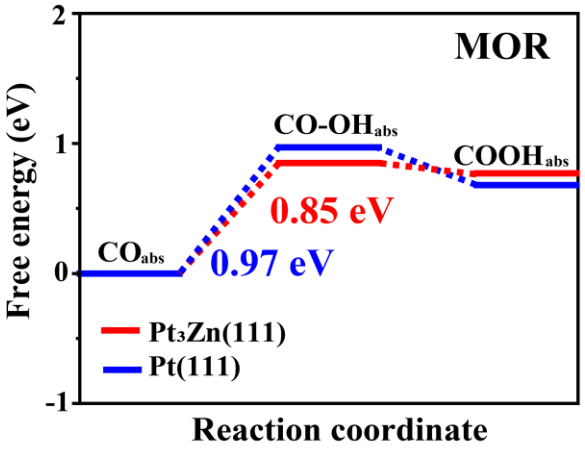

Fig. S19. Gibbs free energy step diagram of the potential-determination-step from CO_{abs} to $CO\text{-}OH_{abs}$ in the MOR transversion on Pt (111) of Pt_3Zn NCs sample for DFT.

Supplementary Tables

Table S1 The elemental loadings of the as-prepared commercial Pt/C catalyst and Pt_3Zn NCs sample by using ICP-OES.

catalyst	ICP (Before Stability test) Loading by weight % relative to the whole sample		ICP (Before Stability test) Loading by atomic % relative to the whole sample		ICP (After Stability test) Loading by weight % relative to the whole sample		ICP (After Stability test) Loading by atomic % relative to the whole sample	
	Pt	Zn	Pt	Zn	Pt	Zn	Pt	Zn
Pt/C	20.28	N/A[a]	1.560	N/A	19.53	N/A	1.490	N/A
Pt_3Zn NCs	12.68	1.46	0.915	0.316	12.62	1.44	0.911	0.312

N/A[a]: not applicable.

Table S2. The percentages of atomic content for C 1s, Pt 4f, N 1s, O 1s, Zn 2p corresponding to the XPS survey spectrum on Pt/C catalyst and Pt_3Zn NCs sample.

Catalysts	Name	C 1s	N 1s	O 1s	Pt 4f	Zn 2p
Pt/C	Atomic%	94.87	N/A[a]	3.57	1.56	N/A
	Weight%	75.92	N/A	3.81	20.28	N/A
Pt_3Zn NCs	Atomic%	91.95	1.77	5.02	0.92	0.34
	Weight%	78.26	1.76	5.69	12.72	1.57

N/A[a]: not applicable.

Table S3. The Zn 2p XPS spectra binding energy and relative ratio of Zn^0, Zn^{2+} for Pt_3Zn NCs catalyst.

Sample	Zn^0		Zn^{2+}	
	Binding energy(eV)	Relative ratio (%)	Binding energy(eV)	Relative ratio (%)
Pt_3Zn NCs	706.15	64.43	711.2	35.57
	719.2		724.3	

Table S4. The Pt 4f XPS spectra binding energy and relative ratio of Pt^0, Pt^{2+}, and Pt^{4+} of Pt/C catalyst and Pt_3Zn NCs sample.

Sample	Pt^0		Pt^{2+}		Pt^{4+}	
	Binding energy(eV)	Relative ratio (%)	Binding energy(eV)	Relative ratio (%)	Binding energy(eV)	Relative ratio (%)
Pt/C	71.41	46.91	74.65	43.39	72.57	9.7
	74.75		75.68		77.6	
Pt_3Zn NCs	71.54	75.98	71.92	15.8	72.73	8.22
	74.5		75.97		77.27	

Table S5. Pt loading obtained from ICP-OES, $ECSA_{CO}$, halfwave potential($E_{1/2}$), mass activity (MA), and specific activity (MA) at 0.9V of Pt/C catalyst and Pt_3Zn NCs sample for ORR before ADT.

Sample	Pt loading (ug)	$ECSA_{CO}$ (m^2/g)	Halfwave potential (V)	Mass activity@0.9V (A/mg_{Pt})	Specific activity@0.9V (mA/cm^2)	Pt loading of catalyst (ICP)
Pt/C	5.0	70.32	0.892	0.23	0.32	20.28%
Pt_3Zn NCs	2.5	54.63	0.945	1.48	2.72	12.72%

Table S6. Pt loading obtained from ICP-OES, $ECSA_{CO}$, halfwave potential($E_{1/2}$), mass activity (MA), and specific activity (MA) at 0.9V of Pt/C catalyst and Pt_3Zn NCs sample for ORR after ADT.

Sample	Pt loading (ug)	$ECSA_{CO}$ (m^2/g)	Halfwave potential (V)	Mass activity@0.9V (A/mg_{Pt})	Specific activity@0.9V (mA/cm^2)	Pt loading of catalyst (ICP)
Pt/C	4.9	78.95	0.841	0.15	0.19	19.53%
Pt_3Zn NCs	2.5	59.78	0.927	1.35	2.25	12.61%

Table S7. Comparisons of the ORR performance in recently published papers.

Catalysts	ECSA (m^2/g)	MA[a] (A/mg_{Pt})	SA[b] (mA/cm^2)	Electrolytes	References
$L1_0$-PtZn-C	61.1	1.02	1.68	0.1 M $HClO_4$	6
PtZn–CoNC	76.1	0.44	N/A[c]	0.1 M $HClO_4$	7
MAC-Pt/ZnFe-N-C	177.62	0.222	0.12	0.1 M $HClO_4$	8
10%-PtZn@NC-800	N/A	0.283	1.03	0.1 M $HClO_4$	9
$L1_0$-PtZn/Zn-NC	81.9	0.926	1.13	0.1 M $HClO_4$	10
PtZn-IMC@NC	62.5	0.808	1.29	0.1 M $HClO_4$	11
d-PtZn/NC	49	0.78	1.6	0.1 M $HClO_4$	12
Pt_3Zn NCs	**54.63**	**1.48**	**2.72**	**0.1 M $HClO_4$**	**This work**

MA[a]: mass activity;

SA[b]: specific activity;

N/A[c]: not applicable.

Table S8. Pt loading obtained from ICP-OES, $ECSA_{CO}$, current density peak, onset potential (V), mass activity (MA), and specific activity (MA) at 0.9V of Pt/C and Pt_3Zn NCs catalysts for MOR, and EOR.

Sample	Pt loading (ug)	$ECSA_{CO}$ (m^2/g)		current density peak ($mA\ cm^{-2}$)		onset potential (V)		MA (A/mg_{Pt}^{-1})		SA (mA/cm^2)	
		MOR	EOR	MOR	EOR	MOR	EOR	MOR	EOR	MOR	EOR
Pt/C	5.0	69.24	70.12	5.10	5.07	0.39	0.42	0.22	0.31	0.20	0.28
Pt_3Zn NCs	2.5	62.38	63.54	20.07	14.77	0.32	0.31	1.69	2.71	1.13	1.78

Table S9 The d band center, Bader charge, charge density difference, PDS, binding energy and adsorption energy of Pt (111) and Pt_3Zn (111) catalyst from DFT.

Sample	d band center (eV)	Bader charge(e)		Charge density difference (e)	PDS (eV)		Binding energy (eV)	Adsorption energy (eV)	
		Pt	Zn		ORR	MOR	CO_{abs}	OH_{abs}	O_{abs}
Pt (111)	-2.57	-0.04	N/A	0.08	1.09	0.97	-1.67	-2.37	-4.15
Pt_3Zn (111)	-2.67	-0.27	0.63	0.15	0.59	0.85	-1.54	-2.45	-4.55

Supplementary References

1 G. Kresse and J. Furthmüller, *Phy. Rev. B*, 1996, **54**, 11169-11186.
2 G. Kresse and J. Furthmüller, *Comput. Mater. Sci.*, 1996, **6**, 15-50.
3 P. E. Blöchl, *Phy. Rev. B*, 1994, **50**, 17953-17979.
4 J. P. Perdew, K. Burke and M. Ernzerhof, *Phys. Rev. Lett.*, 1996, **77**, 3865-3868.
5 L. Zhai, C. Cui, Y. Zhao, X. Zhu, J. Han, H. Wang and Q. Ge, *J. Phys. Chem. C*, 2017, **121**, 16275-16282.
6 J. Liang, Z. Zhao, N. Li, X. Wang, S. Li, X. Liu, T. Wang, G. Lu, D. Wang, B. J. Hwang, Y. Huang, D. Su and Q. Li, *Adv. Energy Mater.*, 2020, **10**, 2000179.
7 L. Zhao, X. Qi, T. Yang, P. Xiong, X. Niu, J. Jiang, Q. Xue, L. Yu, J. S. Chen, A. Cabot and R. Wu, *J. Mater. Chem. A*, 2023, **11**, 24371-24378.
8 J. Li, Q. Zhou, M. Yue, S. Chen, J. Deng, X. Ping, Y. Li, J. Li, Q. Liao, M. Shao and Z. Wei, *Appl. Catal. B Environ. Energy*, 2021, 284, 119728.
9 Y. Xue, H. Li, X. Ye, S. Yang, Z. Zheng, X. Han, X. Zhang, L. Chen, Z. Xie, Q. Kuang and L. Zheng, *Nano Res.*, 2019, **12**, 2490-2497.
10 K. Lee, J. Bak, S. Lee, J. Roh and E. Cho, *ECS Meeting Abstracts*, 2022, **MA2022-01**, 1496.
11 P. Wang, K. Chen, J. Chen, G. Wang, W. Pan and Z. Wen, *Adv. Funct. Mater.*, 2024, DOI: 10.1002/adfm.202408267.
12 W. Yan, S. Cao, H. Liu, Q. Xing, J. Ren, Z. Li, X. Li, X. Lu and Y. Chen, *ACS Appl. Energy Mater.*, 2022, **5**, 13791-13801.